

## The Response of a Uniform Horizontal Temperature Gradient to Heating

MAARTEN H. P. AMBAUM AND PANOS J. ATHANASIADIS

*Department of Meteorology, University of Reading, Reading, United Kingdom*

(Manuscript received 5 August 2005, in final form 12 January 2007)

### ABSTRACT

The response of a uniform horizontal temperature gradient to prescribed fixed heating is calculated in the context of an extended version of surface quasigeostrophic dynamics. It is found that for zero mean surface flow and weak cross-gradient structure the prescribed heating induces a mean temperature anomaly proportional to the spatial Hilbert transform of the heating. The interior potential vorticity generated by the heating enhances this surface response. The time-varying part is independent of the heating and satisfies the usual linearized surface quasigeostrophic dynamics. It is shown that the surface temperature tendency is a spatial Hilbert transform of the temperature anomaly itself. It then follows that the temperature anomaly is periodically modulated with a frequency proportional to the vertical wind shear. A strong local bound on wave energy is also found. Reanalysis diagnostics are presented that indicate consistency with key findings from this theory.

### 1. Introduction

In this paper we examine the linear response of a uniform horizontal temperature gradient to heating. Under certain assumptions on the vertical structure of the heating field, linear perturbations satisfy a modified form of surface quasigeostrophic dynamics. The system is the thermal analog to the Charney–Eliassen system of orographically forced barotropic Rossby waves (Charney and Eliassen 1949; Held 1983) and a surface-only variant of the system studied by Smagorinsky (1953) and Hoskins and Karoly (1981).

The observational motivation to study this problem is the origin of the Northern Hemisphere winter storm tracks where cold continental air flows over a relatively warm ocean and the release of latent and sensible heat appears to kick off local perturbations that provide seeds for downstream baroclinic developments (e.g., Hoskins and Hodges 2002). Furthermore, it has been argued that the structure of the climatological planetary waves follows from the mean heating in these storm tracks. An interesting discussion in earlier literature can be found in Bolin (1950), Bleeker (1950), and Sut-

cliffe (1951). Perhaps, because a simple analytical model exists for orographically induced Rossby waves—it is standard textbook material these days—this became the favored explanation for the climatological planetary waves. However, this model is unsatisfactory for near-surface climatological waves, while it provides only part of the story for the upper air waves. We hope that the present paper provides an analogous simple model for surface temperature waves induced by prescribed heating. The simplicity of our model is very much in the spirit of the Charney–Eliassen model.

The theoretical motivation to study this problem is the peculiar dynamics of linear waves on a uniform surface temperature gradient. Here, the only external parameter is the magnitude of the gradient, which is proportional to the vertical wind shear (units of frequency) through thermal wind balance. From dimensional analysis it then follows that the phase speed of one-dimensional waves has to be proportional to  $k^{-1}$ , with  $k$  the horizontal wavenumber. This implies that the group velocity vanishes so that energy-like quantities, quadratic in the wave field, will have a vanishing flux velocity (e.g., Whitham 1974; Hayes 1977; Straus 1983). It is therefore of particular interest to study the forced problem where wave energy cannot disperse.

The earlier study by Smagorinsky (1953) indicated the importance of the diabatic heating to the mean stationary waves. He added diabatic heating to the baro-

---

*Corresponding author address:* Dr. Maarten Ambaum, Department of Meteorology, University of Reading, P.O. Box 243, Reading, RG6 6BB, United Kingdom.  
E-mail: m.h.p.ambaum@reading.ac.uk

clinic Charney model and solved for the stationary response to heating for an idealized vertical profile. He found a deep baroclinic response, which appeared to have a reasonable realization near the surface when making assumptions about the actual heating field (which was largely unknown at that time). As in the Charney model, the  $\beta$  effect is important in Smagorinsky's setup. However, the assumption of a continuous  $\beta$  is questionable (e.g., Ambaum 1997; Haynes et al. 2001; Swanson 2001) and therefore the deep baroclinic structure of the mean response. Furthermore, the vertical heating profile in Smagorinsky's theoretical study, with vanishing heating at the surface, is perhaps less applicable for the midlatitudes where heating is dominated by the warm ocean surfaces east of the main continents. This has important consequences for the induced potential vorticity structure. Our model does not include a background internal potential vorticity gradient so that vertical coupling of Rossby waves does not occur: even though internal potential vorticity is generated, our model remains essentially a single-layer model and is therefore in spirit similar to the Charney–Eliassen model.

The perturbed temperature gradient we study here is also known as the one-sided Eady wave (e.g., Gill 1982; Davies and Bishop 1994) and forms part of a spectrum of waves supported by the presence of a boundary (Rhines 1970). It is one of the Rossby waves required for baroclinic instability in both the Eady model (Eady 1949) and the Charney model (Charney 1947; Gill 1982; see also Heifetz et al. 2004). Modified versions of these baroclinic instability models have been put forward as models of frontal instability. For example, Joly and Thorpe (1990) have the surface frontal wave interact with internal diabatically produced potential vorticity gradients. Schär and Davies (1990) modify the surface basic state to include a temperature maximum, which is the locus for what should be called a barotropic instability in that the interacting Rossby waves are at the same (surface) level, although there are baroclinic energy conversions in their unstable linear modes. In the present paper these unstable motions are excluded because the only potential vorticity gradient is that associated with the uniform surface temperature gradient, and therefore the Charney–Stern–Pedlosky necessary condition for instability is not met (Bretherton 1966). Müller et al. (1989) study the one-sided Eady wave in semigeostrophic coordinates as a model of cyclogenesis through constructive interference of waves. Some of their results are reproduced in the homogeneous (adiabatic) part of the solution we describe in section 2, although we also find a strong bound on the cycloge-

netic potential of constructive interference through a locally conserved wave energy.

The set of equations that we use are the quasigeostrophic equations with zero initial internal quasigeostrophic potential vorticity but with varying boundary conditions. The flow is unbounded from above and the  $f$  plane and Boussinesq approximations are used. We will use the same scaling as in Held et al. (1995). The streamfunction  $\Psi$ , potential vorticity  $Q$ , potential temperature  $\Theta$ , and velocity field  $(U, V)$  are related as

$$Q = \nabla^2 \Psi, \quad \Theta = \Psi_z, \quad \text{and} \quad (U, V) = (-\Psi_y, \Psi_x). \quad (1)$$

The Laplacian is the three-dimensional Laplacian and subscripts denote partial derivatives. Variables evaluated at the lower surface  $z = 0$  are written in lower case:

$$\theta = \Theta|_{z=0}, \quad \psi = \Psi|_{z=0}, \quad (u, v) = (U, V)|_{z=0}. \quad (2)$$

The equations of motion are

$$Q_t + UQ_x + VQ_y = H_z \quad (3)$$

$$\theta_t + u\theta_x + v\theta_y = h, \quad (4)$$

where  $H$  is a prescribed heating field [this was not included in the equations of Held et al. (1995)] and  $h = H|_{z=0}$ . The system where  $H \equiv 0$  and  $Q \equiv 0$  is called surface quasigeostrophic dynamics or uniform potential vorticity flow.

Like the equation for quasigeostrophic potential vorticity, the equation for surface  $\theta$  is simply advection with, in this case, forcing. However, the dynamics for surface temperature is very different to that of quasigeostrophic potential vorticity. The main difference is a nonlinear instability of small-scale features leading to a highly convoluted surface temperature field with a spectral peak at the smallest scales (e.g., Held et al. 1995). This is the result of the strong singularity in the Green's function for this system (see below). An interesting consequence is that a contour dynamics formulation for surface quasigeostrophic dynamics cannot be practically implemented (D. G. Dritschel 1995, personal communication).

Before we consider the response of a surface temperature gradient to prescribed heating we briefly present the derivation of the Green's function of the system as this is central to the analysis. We will use the interpretation of Bretherton (1966), implying that the system has homogeneous boundary conditions, while surface temperature perturbations are represented as a sheet of potential vorticity with a  $\delta$ -function structure in the vertical. The Green's function then can be applied to both interior and boundary potential vorticity. In this way the contribution to the velocity field of the interior

potential vorticity and the boundary potential vorticity can be separated.

Let us first determine the velocity field due to lower boundary temperature fluctuations only. In this case the interior potential vorticity  $Q = \nabla^2 \Psi$  is identically zero. Streamfunction fields that satisfy the zero potential vorticity condition, as well as the vanishing boundary condition for  $z \rightarrow \infty$ , can be written using a Fourier integral as

$$\Psi = \int \int_{-\infty}^{\infty} \hat{\psi}(k, l) \exp(-|K|z) \exp(ikx + ily) dk dl, \quad (5)$$

with  $K^2 = k^2 + l^2$  and with  $\hat{\psi}(k, l)$  the Fourier transform of the surface streamfunction  $\psi$ . We can then use Eq. (1) to calculate  $\Theta$ :

$$\Theta = \int \int_{-\infty}^{\infty} -|K| \hat{\psi}(k, l) \exp(-|K|z) \exp(ikx + ily) dk dl. \quad (6)$$

By setting  $z = 0$  we get the surface fields. From these we can infer that the Fourier transforms of surface streamfunction  $\psi(x, y)$  and surface potential temperature  $\theta(x, y)$  are related through

$$\hat{\psi}(k, l) = -\frac{\hat{\theta}(k, l)}{|K|}. \quad (7)$$

This then is the spectral representation of the Green's function for the surface temperature field. Compare this with the spectral representation of the Green's function for interior potential vorticity on an infinite or periodic domain:

$$\hat{\Psi}(k, l, m) = -\frac{\hat{Q}(k, l, m)}{|K|^2}, \quad (8)$$

where  $|K|$  is the total three-dimensional wavenumber. This function has strong decay for large wavenumbers, making the velocity field a relatively smooth and non-local transformation of the source field  $Q$ . For a barotropic version of this system (corresponding to  $m = 0$ ) the decay is also quadratic in the total wavenumber. The spectral Green's function for the surface  $\theta$  field decays slower with wavenumber resulting in strongly variable velocity fields at the smallest scales, which are relatively localized around the  $\theta$  anomalies. The velocity field is a derivative of the streamfunction, so each scale in the  $\theta$  field contributes equally to the velocity field. This then leads to the singular behavior at small scales for surface quasigeostrophic dynamics.

In the next section we will present the theory of

forced linear perturbations to a zonally symmetric uniform basic state. In section 3, observational evidence is presented that provides support for the basic setup that we propose in this study. Section 4 contains a concluding discussion on the presented model.

## 2. Linear dynamics of a forced horizontal temperature gradient

We consider a zonally symmetric basic state with forced perturbations. The basic-state zonal velocity  $\bar{U}$  is taken to be

$$\bar{U} = Sz, \quad (9)$$

with  $S$  a constant vertical wind shear. To linear approximation the value of  $S$  will be constant in time as well. The thermal wind relation is equivalent to the definition of potential temperature in terms of the streamfunction. This leads to a basic-state potential temperature profile consistent with the basic-state zonal velocity of

$$\bar{\Theta} = -Sy. \quad (10)$$

This, then, is the baroclinic flow onto which we will produce linear perturbations by applying the heating field  $H$ . The heating field  $H$  is assumed to have zero zonal average, so it will not modify the zonal basic state to linear approximation.

With this basic state the linearized versions of Eqs. (3) and (4) become

$$Q_t + zSQ_x = H_z \quad (11)$$

$$\theta_t - vS = h. \quad (12)$$

We will separate the solution into an inhomogeneous part, denoted by subscript 0, that satisfies

$$zSQ_{0,x} = H_z \quad (13)$$

$$-v_0S = h, \quad (14)$$

and a part that satisfies the homogeneous equations (23) and (24). We have assumed here that the heating field is constant in time. To solve Eqs. (13) and (14) we prescribe an idealized vertical structure of the heating field as follows:

$$\hat{H} = \hat{h}(1 + 2\lambda z) \exp(-2\lambda z), \quad (15)$$

with carets, as before, denoting horizontal Fourier transforms. The vertical decay rate  $\lambda$  is a general function of the horizontal wavenumber  $K$  (below we will set  $\lambda$  to be proportional to  $K$ , implying that the heating depth is proportional to the horizontal scale of the forcing). This particular vertical structure lies between an exponential and a Gaussian. However, it is more real-

istic than the former and in contrast to both these profiles it allows an easy analytical treatment.

Substituting this heating field in Eq. (13) we find

$$ikS\hat{Q}_0 = -4\lambda^2\hat{h} \exp(-2\lambda z). \tag{16}$$

This, then, is the inhomogeneous part of the internal potential vorticity field. The corresponding streamfunction field follows from inversion of the three-dimensional Laplace operator Eq. (1).

The streamfunction can be found by separation of variables, which in spectral space becomes  $\hat{\Psi}_0 = \hat{\psi}_0 p(z)$  where  $p$  satisfies

$$(p'' - K^2 p)\hat{\psi}_0 = \hat{Q}_0 = -\frac{4\lambda^2\hat{h}}{ikS} \exp(-2\lambda z). \tag{17}$$

This equation for  $p$  can be solved by substituting the boundary condition Eq. (14), which in spectral space becomes  $-ik\hat{\psi}_0 S = \hat{h}$ . This way we can eliminate  $\hat{\psi}$  and  $\hat{h}$  and find the following solution for  $p$ :

$$p = \frac{\delta^2}{\delta^2 - 1} \exp(-2\lambda z) - \frac{1}{\delta^2 - 1} \exp(-|K|z), \quad \text{with} \tag{18}$$

$$\delta \equiv \frac{2\lambda}{|K|}.$$

In this solution the boundary conditions  $p(0) = 1$  and  $p(\infty) = 0$  have been used. Note that  $\delta$  is a function of  $K$  and represents the nondimensional inverse heating depth for each wavenumber. The expression for the surface temperature field is  $\hat{\theta}_0 = \hat{\psi}_0 p'(0)$ , which, after some algebra, can be written as

$$\hat{\theta}_0 = -i \frac{|K|}{k} \frac{\hat{h}}{S} \left( 1 + \frac{\delta^2}{1 + \delta} \right). \tag{19}$$

This, then, is the inhomogeneous solution for how the heating field induces a surface temperature anomaly.

This solution can be written particularly elegantly if we assume  $|l| \ll |k|$  and  $\delta = \text{const}$ . The latter condition is equivalent to saying that the heating depth is proportional to the horizontal scale of the heating for the dominant scales in the heating field: this may be reasonable for the latent part of the heating (where water vapor can be distributed deeper, the longer a storm track) and it allows an easy analytical treatment. Similarly, the condition that  $|l| \ll |k|$  is a mathematical assumption to simplify the analysis: we comment on this further in section 4. Using these assumptions we find

$$\hat{\theta}_0 = -i \text{sgn}(k) \frac{\hat{h}}{S} \left( 1 + \frac{\delta^2}{1 + \delta} \right), \tag{20}$$

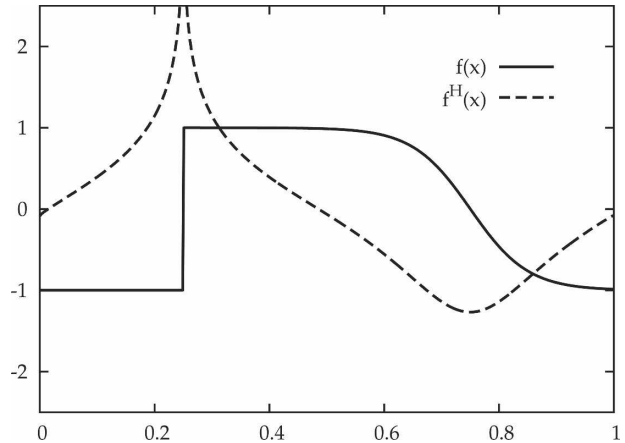


FIG. 1. An example of a periodic function and its Hilbert transform. The Hilbert transform, defined in Eq. (22), has some similarities to a derivative. The Hilbert transform of this function shows a logarithmic divergence at the location of the step.

where  $\text{sgn}(k)$  denotes the sign of  $k$  and  $\delta$  is now a constant real positive number. The factor  $i \text{sgn}(k)$  in Fourier space corresponds to a Hilbert transform in real space (e.g., von Storch and Zwiers 1999).<sup>1</sup> That is,  $\theta_0$  is proportional to minus the spatial Hilbert transform of  $h$ :

$$\theta_0 = -\frac{h^H}{S} \left( 1 + \frac{\delta^2}{1 + \delta} \right). \tag{21}$$

The Hilbert transform of a function has some similarity to its derivative, as can be seen in its spectral representation: a cosine is transformed into minus a sine and a sine is transformed into a cosine. The product of  $\hat{h}$  with  $i \text{sgn}(k)$  in Fourier space corresponds to the convolution in real space:

$$h^H(x) = \frac{1}{\pi} \int_{-\infty}^{\infty} \frac{h(x + \xi)}{\xi} d\xi, \tag{22}$$

where the integral is a principal value integral. From this convolution the similarity between the Hilbert transform and the derivative of a function also stands out. Figure 1 shows an example of a Hilbert transform for an idealized periodic function.

The inhomogeneous solution Eq. (21) can be interpreted as follows: a cold perturbation will occur where there is a strong positive heating gradient in the  $x$  direction. Because of Eq. (14) we find meridional winds proportional and opposite to the heating field: northward winds ahead of the cold anomaly and southward

<sup>1</sup> Note that in von Storch and Zwiers (1999) the definitions of Fourier and Hilbert transforms both have a reverse sign for frequencies.

winds behind the anomaly. The compensation between meridional temperature advection and heating is typical for midlatitudes. This situation corresponds to the shallow heating case, as discussed in Hoskins and Karoly (1981). The factor with the  $\delta$  in Eq. (21) corresponds to the contribution to the temperature anomaly due to the interior potential vorticity; if  $\delta = 0$  (i.e.,  $\lambda = 0$ ), the interior potential vorticity in Eq. (16) vanishes. The interior potential vorticity is opposite in sign to the surface potential vorticity implied by the temperature anomalies. This means that the interior potential vorticity reduces the surface winds corresponding to the surface temperature anomalies alone. Then, according to Eq. (14), a larger temperature anomaly is required to provide the winds that can balance the heating field.

Next we turn our attention to the homogeneous part of the solution to Eqs. (11) and (12). We denote the homogeneous solution with subscript 1, so all fields  $f$  are now written as  $f = f_0 + f_1$ . The homogeneous part satisfies

$$Q_{1,t} + zSQ_{1,x} = 0 \tag{23}$$

$$\theta_{1,t} - v_1S = 0. \tag{24}$$

This set of equations is exactly identical to linearized surface quasigeostrophic dynamics because, if the initial  $Q_1$  is chosen to be zero, it remains zero. Equation (24) is then the only dynamical equation to be considered. It is easiest to consider the fields initially in spectral space. We then find, using Green's function for surface quasigeostrophic dynamics, Eq. (7):

$$\hat{v}_1 = ik\hat{\psi}_1 = -i\frac{k}{|K|}\hat{\theta}_1. \tag{25}$$

This equation can be rewritten elegantly if we again assume  $|l| \ll |k|$  in which case we find

$$\hat{v}_1 = -i \operatorname{sgn}(k)\hat{\theta}_1$$

or

$$v_1 = -\theta_1^H. \tag{26}$$

Under the assumption of meridionally extended perturbations we then find the following closed equation for the surface temperature field:

$$\theta_{1,t} + S\theta_1^H = 0. \tag{27}$$

Hilbert transforms have the property that  $(f^H)^H = -f$  (making it in some sense a real representation of the imaginary number  $i$ ). Furthermore, the spatial Hilbert transform commutes with a time derivative,  $(f_t)^H =$

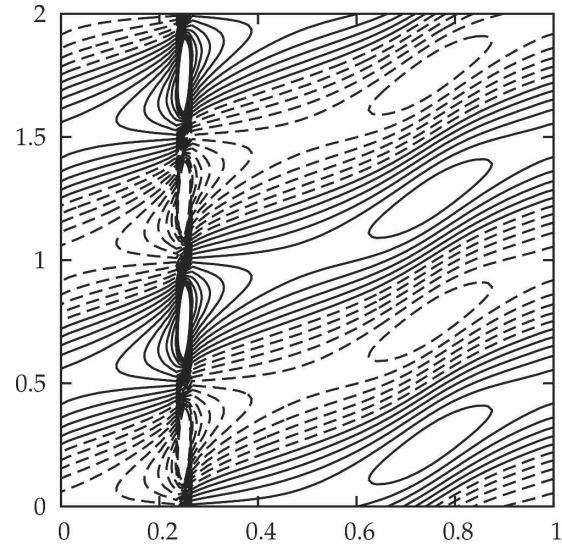


FIG. 2. Hovmöller diagrams showing the  $\theta_1$  field evolution according to Eq. (27) with initial condition of the shape of the example function in Fig. 1. Time along the vertical axis is in units of one period. Solid contours correspond to positive values, dashed contours to negative values, and the contour interval is 0.2 (not drawn above values of 2.5).

$(f^H)_t$ . Using these properties we can take the Hilbert transform of Eq. (27) to find

$$\theta_{1,tt} + S^2\theta_1 = 0. \tag{28}$$

This means that the  $\theta_1$  field is periodic everywhere with angular frequency  $S$ . It is an interesting aspect of the Hilbert transform that, even though the  $\theta_1$  tendency field according to Eq. (27) is a nonlocal function of the  $\theta_1$  field, the tendency is such that the evolution of  $\theta_1$  is periodic with the same period at all locations.<sup>2</sup> From Eq. (28) it then follows that the general solution for  $\theta_1$  must be of the form  $\theta_1 = A(x) \cos(St) + B(x) \sin(St)$ . The functions  $A$  and  $B$  follow from the initial condition on  $\theta_1$  and from its initial tendency, which can be calculated from Eq. (27). The general result is

$$\theta_1(x, t) = \theta_1(x, 0) \cos(St) - \theta_1^H(x, 0) \sin(St). \tag{29}$$

Figure 2 shows an example of the evolution for an initial condition on  $\theta_1$  of a similar shape to the Hilbert transform example of Fig. 1 [it is analogous to Fig. 2 in the Müller et al. (1989) paper]. The anomalies always propagate “eastward” with local perturbations varying periodically.

As alluded to in the introduction, the wave energy

<sup>2</sup> This peculiar property of the system would be the case for every functional  $\mathcal{F}$ , which commutes with time differentiation and which has the property that  $\mathcal{F}(\mathcal{F}f) = -f$  for any function  $f$ .

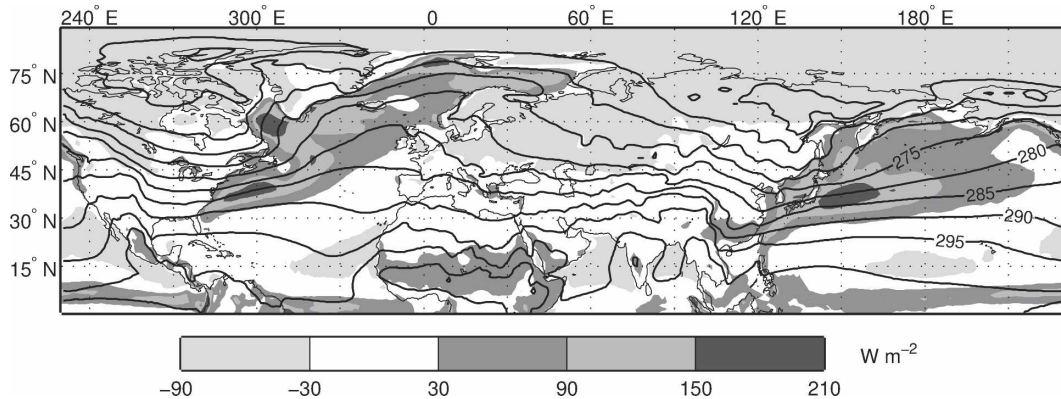


FIG. 3. DJFM climatologies. Contours show potential temperature at 925 hPa ( $\theta_{925}$ ) and the shading the diabatic heating integral from the surface to 700 hPa ( $\mathcal{H}$ ). The contouring and shading intervals are 5 K and  $60 \text{ W m}^{-2}$ , respectively.

does not disperse in this model. Here we can set the wave energy to be proportional to  $\theta_1^2 + (\theta_1^H)^2$  (e.g., von Storch and Zwiers 1999; Zimin et al. 2003). We can then use Eq. (27) to deduce that this wave energy remains locally conserved:

$$\frac{\partial}{\partial t} (\theta_1^2 + (\theta_1^H)^2) = 0. \quad (30)$$

In Fig. 2 this can be clearly seen: the wave energy is stuck at the same “longitude.” This local conservation of wave energy puts a strong bound on the cyclogenetic potential of constructive interference, a mechanism suggested by Müller et al. (1989). Incidentally, Müller et al. also note the strictly periodic behavior of their wave solutions, as in Eq. (28).

In the next section we will examine some observational evidence for the results in Eqs. (21) and (29).

### 3. Observational evidence

The simplified dynamics as presented in the previous section has some salient features that can be summarized as follows:

- (i) the zonal structure of the inhomogeneous zonal anomaly temperature  $\theta_0$  is proportional to the Hilbert transform of the zonal structure of the heating field [Eq. (21)],
- (ii) the tendency of the homogeneous temperature anomaly  $\theta_1$  is proportional to the spatial Hilbert transform of the anomaly itself [Eq. (27)],
- (iii) the homogeneous temperature anomaly  $\theta_1$  varies harmonically with a period inversely proportional to the vertical wind shear [Eq. (29)].

We test these theoretical results in a suitable domain of the Northern Hemisphere. Given that temporal vari-

ability is not determined alone by the dynamics described here (there are also baroclinic waves acting at the same time scales), emphasis is given to the time mean solution, which appears to be of greater interest. However, even for the latter, the effects of large-scale orography and the simplifications of the theory cannot be overlooked.

The dataset used for this analysis consists of two parts:

- 1) Monthly climatologies (1979–2001) based on the ECMWF reanalysis for temperature and other fields at 925 hPa and the diabatic heating integral from the surface to 700 hPa from the 40-yr ECMWF Reanalysis (ERA-40) Atlas (Kållberg et al. 2005). This integral (units of  $\text{W m}^{-2}$ ) is denoted by  $\mathcal{H}$  to distinguish it from  $h$ , the theoretical heating rate at the surface (units of  $\text{K s}^{-1}$ ). From these data the corresponding December–March (DJFM) climatologies were obtained.
- 2) Six-hourly potential temperature at  $\sigma = 0.995$  ( $\theta_{\text{srf}}$ ) from the National Centers for Environmental Prediction–National Center for Atmospheric Research (NCEP–NCAR) reanalysis for 56 DJFM seasons (December 1948–March 2004) with a spatial resolution of  $2.5^\circ \times 2.5^\circ$ .

Clearly, the assumptions of a uniform meridional potential temperature gradient basic state with perturbations that have weak meridional structure are only partially met in the real atmosphere. Figure 3 shows the DJFM climatologies of  $\mathcal{H}$  and potential temperature at 925 hPa ( $\theta_{925}$ ). Two maxima of diabatic heating can be seen (shading) next to the eastern coasts of Asia and North America; vigorous surface dynamics occurs there (Hoskins and Hodges 2002). In the latitude zone  $40^\circ$ – $50^\circ\text{N}$  the temperature gradient is strong and less af-

ected by the Rockies and the Himalayas lying more to the south. All variables have been averaged over this latitude range so that spatial variations are restricted to the  $x$  direction (longitude) only and this one-dimensional, periodic domain permits a straightforward calculation of Hilbert transforms.

Equation (21) was examined using the climatologies of  $\theta_{925}$  and  $\mathcal{H}$ . Heating rate is assumed to follow Eq. (15). In this case Eq. (21) becomes in dimensional quantities (denoted with an asterisk)

$$\theta_0^* = - \left[ \frac{\theta^* g}{S^* c_p T^* \Delta p^*} \left( 1 + \frac{\delta^2}{1 + \delta} \right) \right] \mathcal{H}'^H, \quad (31)$$

where  $\Delta p^*$  is the thickness of the heating profile in pressure units and  $S^*$ ,  $\theta^*$ ,  $T^*$  are taken as weighted spatial and time averages; primes denote zonal anomalies. We will use the time mean  $\mathcal{H}'$  so that  $\theta_0^*$  corresponds to the time mean of  $\theta'_{925}$ . Using thermal wind balance we can write  $S^*$  as

$$S^* = \frac{f}{N} \left( \frac{dU^*}{dz} \right) = \frac{g}{N\theta^*} \left( \left| \frac{d\theta^*}{dy} \right| \right), \quad (32)$$

where  $N$  is the Brunt–Väisälä frequency. An estimate for  $\delta$  can be obtained through Eq. (18) by taking  $\delta = f/(|k^*|D^*N)$ , where  $D^*$  is the depth corresponding to  $\Delta p^*$  and  $k^*$  the wavenumber approximated to fit double the zonal width of one of the heating peaks (leading to a value of  $2\pi/k^* \approx 8000$  km; see Fig. 4). Combining these estimates one can get a value for the constant of proportionality within the brackets in Eq. (31). This is clearly sensitive to some of the choices one has to make, especially for the depth scale of the heating. If one takes  $\Delta p^* = 200$  hPa (e.g., Källberg et al. 2005), the corresponding value for the constant of proportionality turns out to be about  $0.1 \text{ K (W m}^{-2}\text{)}^{-1}$ . Figure 4 shows  $\theta'_{925}$  (solid line) and  $-\mathcal{H}'^H$  (dashed line). The two lines match to a remarkable degree as predicted by the theory of Eq. (21) and its dimensional counterpart in Eq. (31) with the correct constant of proportionality. Both profiles exhibit a minimum close to the Asian and North American eastern coastlines, which are indicated by gray shading in this and subsequent plots. Cold anomalies occur where the strong positive heating gradients are. On the large scale there is a good correspondence between the two profiles. On the smaller scales the correspondence is weaker, although some small-scale features in the heating anomalies (e.g., at the North American northwest coast:  $240^\circ\text{E}$ ; the Great Lakes:  $275^\circ\text{E}$ ; and Japan:  $135^\circ\text{E}$ ) appear to be reflected in the temperature profile.

Another model result that has been examined is that the tendency of the temperature anomaly  $\theta_1$  is propor-

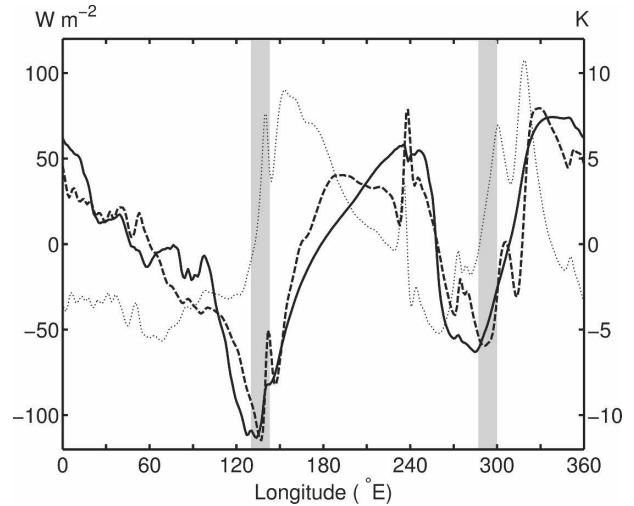


FIG. 4. Zonal anomalies of DJFM climatologies averaged in  $40^\circ$ – $50^\circ\text{N}$ . Solid line represents potential temperature at 925 hPa ( $\theta'_{925}$ ), thin dotted line diabatic heating below 700 hPa ( $\mathcal{H}'$ ), and dashed line minus its Hilbert transform ( $-\mathcal{H}'^H$ ). Gray bars indicate the eastern coastlines of Asia and North America in the selected latitude zone.

tional to the spatial Hilbert transform of the anomaly itself with the constant of proportionality being the vertical wind shear [Eq. (27)]. To check against observations the correlation coefficient between  $\theta_{1,t}$  and  $\theta_1^H$  is calculated. Potential temperature near the surface (6-hourly  $\theta_{\text{srf}}$ ) is used to represent  $\theta_1$ . To exclude the dominant diurnal cycle a low-pass Fourier filter is applied to the time series retaining periods longer than 1.5 days. Also, the DJFM mean is removed for each individual season, and finally averaging in the latitude zone leaves a single spatial dimension ( $0^\circ$ – $360^\circ\text{E}$ ). From Eq. (27)  $\theta_{1,t}$  and  $\theta_1^H$  are expected to be anticorrelated. This should be the case for both correlation in time and space. Calculating the spatial correlation at each time step and averaging over the whole period (56 seasons  $\times$  121 days  $\times$  4 daily) led to a spatial correlation of about  $-0.80$ . The temporal correlation is plotted as a function of longitude in Fig. 5. The shading indicates again the coastlines, which closely coincide with maxima of the heating gradient. The anticorrelation is generally strong, better than  $-0.7$  at most longitudes. The long time series adds statistical significance to this positive result. Anticorrelation shows minima where the westerly flow meets the continents ( $240^\circ$  and  $360^\circ\text{E}$ ), although this appears not to have an obvious reason.

A Hovmöller plot of  $\theta_1(x, t)$ , as represented by 6-hourly  $\theta_{\text{srf}}$ , is shown in Fig. 6, revealing fairly coherent moving anomalies with a phase speed of about  $15 \text{ m s}^{-1}$ . This appears to be a dominant characteristic of the variability throughout the whole data period out-

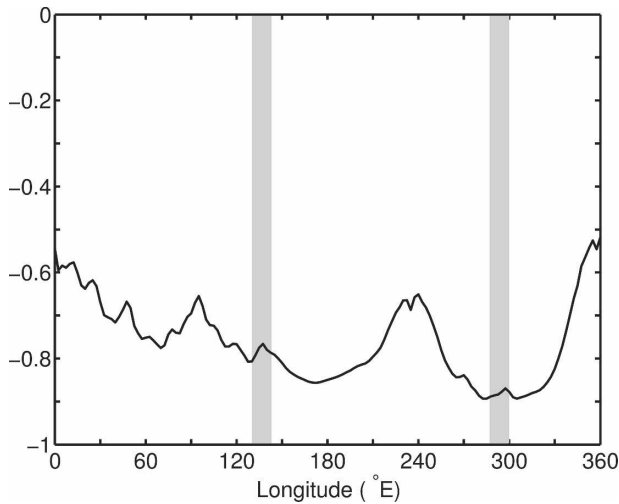


FIG. 5. Temporal correlation coefficient between the tendency and the spatial Hilbert transform of  $\theta'_{\text{srf}}$  averaged over the 40°–50°N latitude band. DJFM means and periods shorter than 1.5 days have been removed. Shading as in Fig. 4.

side the diurnal variability band. This gives weight to the theoretical results of Eqs. (27) and (28) over the default explanation that the observed anticorrelation (Fig. 5) is rather explained by simple advection (given that the Hilbert transform and spatial derivative exhibit quite a strong similarity): the average low-level westerly flow cannot match this high phase speed. There also seems to be consistency with a local conservation of wave energy, as noted in the discussion of Eq. (30), especially at the east coast of the United States. Clearly, this is also an area of vigorous baroclinic cyclogenesis bound to the coastline, which would provide an alternative explanation of the localization of the wave energy.

#### 4. Conclusions

Small perturbations on a homogeneous horizontal temperature gradient, with weak surface winds and modified by a heating field with weak cross-gradient structure, satisfy a simple, two-dimensional (time and zonal direction) set of equations: Eq. (21) for the time mean and Eq. (27) for the anomaly. In other words, the mean surface temperature anomaly is proportional to the spatial Hilbert transform of the heating, and the tendencies are proportional to the spatial Hilbert transform of the anomaly itself, leading to a frequency proportional to the basic-state temperature gradient. Although various assumptions are used to derive these results, we have shown that observed zonal temperature anomalies to a quite large extent satisfy these properties.

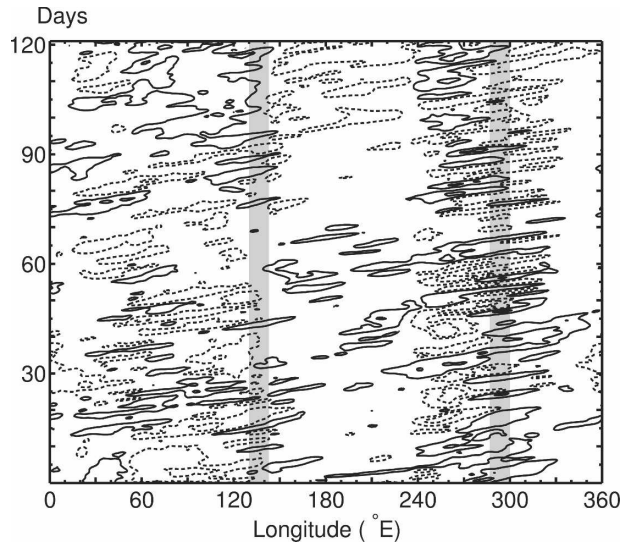


FIG. 6. Hovmöller diagram of  $\theta'_{\text{srf}}$  averaged over the 40°–50°N latitude band for December 1996–March 1997. Contour interval is 8 K, dashed for negatives. Shading as in Fig. 4. The phase speed is about 15 m s<sup>-1</sup>.

The assumption of weak meridional structure (i.e., ignoring  $l$  compared to  $k$ ) will modify the system. Linear unforced waves will attain a nonzero group velocity. From the derivation of Eq. (26) it can be seen that in the presence of meridional structure the meridional wind and surface temperature anomaly would be related by something like a desingularized Hilbert transform. In fact, for a temperature field with a dominant scale in both  $x$  and  $y$  directions the meridional wavenumber introduces a modification involving a nearly constant factor proportional to  $L_x/L_y$ , with  $L_x$  and  $L_y$  the scales in the  $x$  and  $y$  directions. It is therefore expected that most of the qualitative character of the Hilbert transform relationship is retained. The purely periodic character, as expressed by Eq. (28), will also be modified. Similar considerations hold for the derivation of Eq. (21). Equation (19) is the more general version, allowing meridional structure, but it does not allow the compact expression in terms of Hilbert transforms.

A surface zonal wind can be easily included in Eq. (27). However, the Doppler shift due to observed climatological zonal wind was shown to be weak compared to the main periodicity of the system. The observed zonal propagation of temperature anomalies (see Fig. 6) cannot be explained by zonal advection, and the surface Rossby wave character as implied in Eq. (27) is essential for this propagation. However, some of the waves in Fig. 6 are baroclinic waves, which are expected to propagate with the zonal wind speed at the steering level. This would also fit the observed phase speed. In fact, regression analyses on complex EOFs of

the surface temperature fields (not shown) indicated that some of the waves had upward propagating characteristics, a process for which interior potential vorticity gradients are necessary.

Clearly, the assumption of vanishing interior potential vorticity gradients is expected to be only weakly satisfied in the atmosphere. Interior potential vorticity gradients associated with the jet stream have to be at higher altitude than the  $e$ -folding depth corresponding to the dominant wavenumber of the temperature anomalies to ensure effective decoupling of the surface temperature wave and the jet. Also, diabatic heating can induce interior potential vorticity gradients, for example, as described in Joly and Thorpe (1990).

The exclusion of potential vorticity gradients other than that associated with the surface temperature gradient precludes linear quasigeostrophic instability in our system. It is, however, of interest to note the strongly singular behavior of surface quasigeostrophic dynamics and it may be possible that our system admits finite amplitude instabilities with linear precursors as alluded to in Müller et al. (1989). This could be an alternative paradigm for frontal wave development and is an area of current research.

Despite its apparent shortcomings, the present model appears to perform fairly well when confronted with analysis data. The spirit of the model was to provide the thermal analog to the textbook Charney–Eliassen model for orographically induced Rossby waves with the same level of simplicity.

*Acknowledgments.* P.J.A. was supported by a postgraduate scholarship from the Greek State Scholarships Foundation (IKY). Two anonymous reviewers and the editor have contributed substantially to the final version of the manuscript by urging the authors to seek explicit solutions including the interior potential vorticity. We also thank one of the reviewers for pointing out the work by Müller et al.

#### REFERENCES

- Ambaum, M. H. P., 1997: Isentropic formation of the tropopause. *J. Atmos. Sci.*, **54**, 555–568.
- Bleeker, W., 1950: The structure of weather systems. *Centenary Proceedings of the Royal Meteorological Society 1950*, R. Watson-Watt, Ed., Royal Meteorological Society, 66–80.
- Bolin, B., 1950: On the influence of the earth's orography on the general character of the westerlies. *Tellus*, **2**, 184–195.
- Bretherton, F. P., 1966: Critical layer instability in baroclinic flows. *Quart. J. Roy. Meteor. Soc.*, **92**, 325–334.
- Charney, J. G., 1947: The dynamics of long waves in a baroclinic westerly current. *J. Meteor.*, **4**, 135–162.
- , and A. Eliassen, 1949: A numerical method for predicting the perturbations of the middle latitude westerlies. *Tellus*, **1**, 38–54.
- Davies, H. C., and C. H. Bishop, 1994: Eady edge waves and rapid development. *J. Atmos. Sci.*, **51**, 1930–1946.
- Eady, E. T., 1949: Long waves and cyclone waves. *Tellus*, **1**, 33–52.
- Gill, A. E., 1982: *Atmosphere–Ocean Dynamics*. Academic Press, 662 pp.
- Hayes, M., 1977: A note on group velocity. *Proc. Roy. Soc. London*, **354**, 533–535.
- Haynes, P., J. Scinocca, and M. Greenslade, 2001: Formation and maintenance of the extratropical tropopause by baroclinic eddies. *Geophys. Res. Lett.*, **28**, 4179–4182.
- Heifetz, E., C. H. Bishop, B. J. Hoskins, and J. Methven, 2004: The counter-propagating Rossby-wave perspective on baroclinic instability. I: Mathematical basis. *Quart. J. Roy. Meteor. Soc.*, **130**, 211–231.
- Held, I. M., 1983: Stationary and quasi-stationary eddies in the extratropical troposphere: Theory. *Large-Scale Dynamical Processes in the Atmosphere*, B. J. Hoskins and R. Pearce, Eds., Academic Press, 127–168.
- , R. T. Pierrehumbert, S. T. Garner, and K. L. Swanson, 1995: Surface quasi-geostrophic dynamics. *J. Fluid Mech.*, **282**, 1–20.
- Hoskins, B. J., and D. J. Karoly, 1981: The steady linear response of a spherical atmosphere to thermal and orographic forcing. *J. Atmos. Sci.*, **38**, 1179–1196.
- , and K. I. Hodges, 2002: New perspectives on the Northern Hemisphere winter storm tracks. *J. Atmos. Sci.*, **59**, 1041–1061.
- Joly, A., and A. J. Thorpe, 1990: Frontal instability generated by tropospheric potential vorticity anomalies. *Quart. J. Roy. Meteor. Soc.*, **116**, 525–560.
- Källberg, P., P. Berrisford, B. J. Hoskins, A. Simmons, S. Uppala, S. Lamy-Thépaut, and R. Hine, 2005: ERA-40 Atlas. ERA-40 Project Report Series 19, ECMWF, 191 pp.
- Müller, J. C., H. C. Davies, and C. Schär, 1989: An unsung mechanism for frontogenesis and cyclogenesis. *J. Atmos. Sci.*, **46**, 3664–3672.
- Rhines, P., 1970: Edge-, bottom-, and Rossby waves in a rotating stratified fluid. *Geophys. Fluid. Dyn.*, **1**, 273–302.
- Schär, C., and H. C. Davies, 1990: An instability of mature cold fronts. *J. Atmos. Sci.*, **47**, 929–950.
- Smagorinsky, J., 1953: The dynamical influence of large-scale heat sources and sinks on the quasi-stationary mean motions of the atmosphere. *Quart. J. Roy. Meteor. Soc.*, **79**, 342–366.
- Straus, D. M., 1983: Conservation laws of wave action and potential enstrophy for Rossby waves in a stratified atmosphere. *Pure Appl. Geophys.*, **121**, 917–946.
- Sutcliffe, R. C., 1951: Mean upper contour patterns of the Northern Hemisphere—The thermal-synoptic view-point. *Quart. J. Roy. Meteor. Soc.*, **77**, 435–440.
- Swanson, K. L., 2001: Upper-tropospheric potential vorticity fluctuations and the dynamical relevance of the time mean. *J. Atmos. Sci.*, **58**, 1815–1826.
- von Storch, H., and F. W. Zwiers, 1999: *Statistical Analysis in Climate Research*. Cambridge University Press, 484 pp.
- Whitham, G. B., 1974: *Linear and Nonlinear Waves*. John Wiley and Sons, 636 pp.
- Zimin, A. V., I. Szunyogh, D. J. Patil, B. R. Hunt, and E. Ott, 2003: Extracting envelopes of Rossby wave packets. *Mon. Wea. Rev.*, **131**, 1011–1017.